# Supplementary Information

## Different Pathways for Cr(III) Oxidation: Implications for Cr(VI) Reoccurrence in Reduced Chromite Ore Processing Residue

Weizhen Liu[†,‡,⊥], Jing Li[†,‡,⊥], Jiayi Zheng[†,‡], Yao Song[†], Zhenqing Shi[†], Zhang Lin*[,†,‡], Liyuan Chai[§]

[†] *School of Environment and Energy, Guangdong Provincial Key Laboratory of Solid Wastes Pollution Control and Recycling, South China University of Technology, Guangzhou, Guangdong 510006, P. R. China*

[‡] *The Key Laboratory of Pollution Control and Ecosystem Restoration in Industry Clusters (Ministry of Education), Guangzhou, Guangdong 510006, P. R. China*

[§] *School of Metallurgy and Environment, Central South University, Changsha 410083, P. R. China*

*Corresponding author: Phone: 86-020-39380503; E-mail: zlin@scut.edu.cn*

*382 Zhonghuan Road East, Guangzhou Higher Education Mega Centre, Guangzhou 510006, P. R. China*

[⊥]*These authors contributed equally to this work.*

# 1. Experimental details

## 1.1 Synthesis of Cr(OH)$_{3(s)}$ and δ-MnO$_{2(s)}$

Cr(NO$_3$)$_3$·9H$_2$O and Mn(NO$_3$)$_2$·4H$_2$O were used for the synthesis of Cr(OH)$_{3(s)}$ and δ-MnO$_{2(s)}$, respectively. Cr(OH)$_{3(s)}$ was synthesized according to the method described by Lee and Hering[1] with a modification. Although stirring vigorously, 1.0 M NaOH was slowly added to 600 mL of the Cr(III) stock solution (60 mM) until the solution pH reached 9. After aging for 4 h, the suspension was centrifuged, and the solids were washed three times and subsequently freeze dried. Synthetic δ-MnO$_2$ was prepared by the reaction between KMnO$_4$ and Mn(NO$_3$)$_2$·4H$_2$O at a basic pH following the method described by Villalobos et al.[2] Finally, the formed Cr(OH)$_{3(s)}$ and δ-MnO$_{2(s)}$ were collected for the following characterization, as shown in Figure S1-S2 and Table S1-S2. All the chemical reagents were of analytical grade and used without further treatment. Deionized water was used throughout the experiments.

## 1.2 Oxidation experiments

Three series of experiments were carried out at pH 9–11: (1) Cr(OH)$_3$ suspension under oxic and anoxic conditions, (2) Cr(OH)$_3$ suspension with 10 mg/L δ-MnO$_2$ under oxic and anoxic conditions, and (3) Cr(OH)$_3$ suspension with 0.2 mM Mn(NO$_3$)$_2$·4H$_2$O stock solution under oxic conditions. All the experiments were performed in 500 mL serum bottles with 350 mL of Cr(OH)$_3$ suspension stirred with polypropylene-coated stir bars at a speed of 400 rpm on a multi-position stirrer at room temperature. The Cr(OH)$_3$ suspension was prepared by adding the above synthetic Cr(OH)$_{3(s)}$ (500 mg/L, namely 4.85 mM initial Cr(III) concentration) into alkaline solution with 50 mM NaNO$_3$ and 50 mM pH buffer. Background electrolyte (50 mM NaNO$_3$) was used in all experiments to maintain ionic strength. The solution pH was adjusted with 1.0 M NaOH and 1.0 M HNO$_3$, and the pH was maintained with the buffers: CHES for pH 9 and CAPS for pH 10 and 11. The oxidation experiments performed in an atmospheric environment were considered as the oxic condition. For the anoxic condition, the water was purged with N$_2$ for approximately 2 h before experiments, and the experiments were performed in an anaerobic glove box with serum bottles sealed with rubber stoppers. Samples (2.5 mL) were collected at certain intervals through the stopper by a syringe needle and filtered with 0.02 μm polyethersulfone syringe filters (ether sulfone) for the following analysis of dissolved Cr(VI) and Mn(II) concentrations.

**1.3 Adsorption experiments of Cr(VI) and Mn(II) on the solids**

Cr(VI) absorption: 60 mL of 0.5 mg/L $NaCr_2O_4$ solution was prepared with deionized water, and it was evenly divided into 6 bottles of 10 mL (with each 2 bottles of pH 9, 10, and 11). Subsequently, 0.02 g $Cr(OH)_{3(s)}$ and 0.02 g $\delta-MnO_{2(s)}$ were added in the $NaCr_2O_4$ solution of each 2 bottles with the same pH, respectively, with stirring vigorously for about 48 h under anoxic condition. The solutions were collected by centrifugal separation for testing the Cr(VI) concentration.

Mn(II) absorption: 30 mL of 10 mg/L $Mn(NO_3)_2$ solution was prepared with deionized water, and it was evenly divided into 3 bottles of 10 mL with pH of 9, 10, and 11). Subsequently, 0.02 g $\delta-MnO_{2(s)}$ was added in each $Mn(NO_3)_2$ solution, with stirring vigorously for about 48 h under anoxic condition. The solutions were collected by centrifugal separation for testing the Mn(II) concentration. The Cr(VI) and Mn(II) concentrations in each solution were determined and shown as Table S3.

**1.4 Cr(OH)₃ dissolution experiments in alkaline solution**

500 mg/L of $Cr(OH)_{3(s)}$ was added into 350 mL alkaline solution with pH range from 8 to 12. After stirring vigorously for about 96 h under anoxic condition, the solution samples (10 mL) were taken by syringe needles and filtered with 0.02 μm ether sulfone for determination of Cr concentration. The total concentration of dissolved Cr is shown in Figure S3.

**1.5 Analysis and characterization**

The Cr(VI) concentrations were measured by the diphenylcarbazide colorimetric method[3] with a UV–vis spectrophotometer (UV2600, Shimadzu) with a Cr(VI) detection limit of 0.04 mg/L. Total dissolved Cr and Mn concentrations were measured by inductively coupled plasma–optical emission spectrometry (ICP-OES, AVIO 200, PerkinElmer). The synthetic $Cr(OH)_{3(s)}$ and $\delta-MnO_{2(s)}$ and the solid products of Cr(III) oxidation experiments were characterized by X-ray diffraction (XRD), X-ray photoelectron spectroscopy (XPS), scanning electron microscopy (SEM). Their specific surface areas of synthetic samples were determined by the Brunauer–Emmett–Teller (BET) method with Micromeritics ASAP 2020 based on adsorption isotherms of nonreactive $N_2(g)$. XRD was conducted using Cu Kα radiation with an X-ray diffractometer (Advance D8, Bruker) to determine crystal phases of the products. The valence of Mn on the solid surface was determined by analyzing the solid products using XPS (Escalab

250Xi, Thermo Fisher Scientific) with an Al Kα X-ray source at 30.0 eV pass energy at a 500 μm X-ray spot size. The binding energy was calibrated using C1s at 284.6 eV. The Mn $2p_{3/2}$ spectrum was divided into five multiplet peaks (total of 15 binding energies) of Mn(IV), Mn(III), and Mn(II) according to the literature.[4]

Mn K-edge XANES spectroscopy together with PCA and LCF analyses were used for characterization and quantitation of Mn species in the solid products. The Mn(II, III, and IV) standards (analytical grade or better)—$Mn_2O_3$, MnO, $MnCO_3$, $MnCl_2$, $Mn(NO_3)_2$, and $MnO_2$—were purchased from Aladdin. Pyrolusite (β-$MnO_2$), feitknechtite (β-MnOOH), hausmannite ($Mn_3O_4$), bixbyite ($Mn_2O_3$), ramsdellite (γ-$MnO_2$), and birnessite ($Na_{0.7}Ca_{0.3}Mn_7O_{14}·2.8H_2O$) were synthesized according to the previously published methods.[3, 5] The XANES data were collected at the beamline 1W1B at the Beijing Synchrotron Radiation Facility and analyzed with the software Athena.[6]

## 2. Results
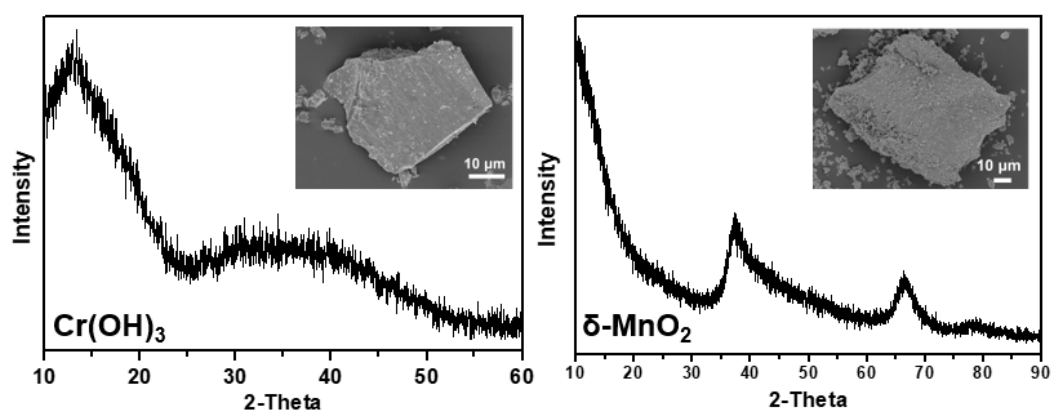
### 2.1 Characteristics of synthetic reactants



**Figure S1.** XRD patterns of synthetic $Cr(OH)_3(s)$ and δ-$MnO_2$ with their SEM photos inserted.
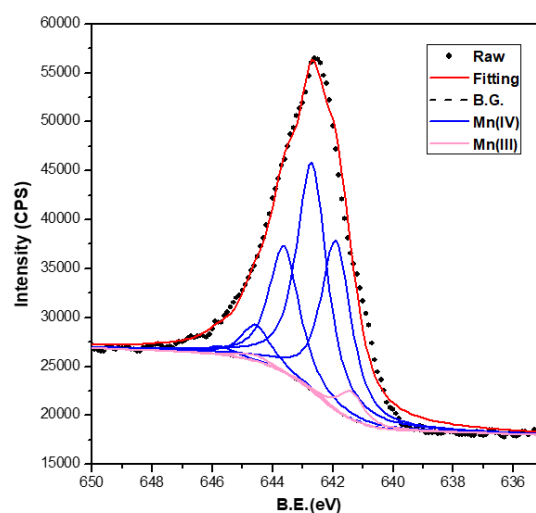
**Figure S2.** XPS spectra of Mn 2p$_{3/2}$ photoelectron lines for the synthetic δ-MnO$_2$.

**Table S1.** Binding energies (BE) of surface Mn species for fitting the Mn2p$_{3/2}$ peak of the synthetic δ-MnO$_2$ and the relative area of each multiplet for the surface species.

| surface species | BE (eV) | FWHM (eV) | Percent (%) |
|---|---|---|---|
| Mn(IV)-O multiplet 1 | 641.9 | 1.2 | 28.28 |
| Mn(IV)-O multiplet 2 | 642.75 | 1.2 | 38.03 |
| Mn(IV)-O multiplet 3 | 643.62 | 1.2 | 20.98 |
| Mn(IV)-O multiplet 4 | 644.72 | 1.2 | 6.02 |
| Mn(IV)-O multiplet 5 | 645.75 | 1.2 | 1.39 |
| Mn(IV)-O overall: 94.71 (%) | | | |
| Mn(III)-O multiplet 1 | 640.70 | 1.5 | 0.02 |
| Mn(III)-O multiplet 2 | 641.40 | 1.5 | 3.85 |
| Mn(III)-O multiplet 3 | 642.21 | 1.5 | 0.41 |
| Mn(III)-O multiplet 4 | 643.23 | 1.5 | 0.04 |
| Mn(III)-O multiplet 5 | 644.60 | 1.5 | 0.97 |
| Mn(III)-O overall: 5.29 (%) | | | |
| Mn Average Oxidation State (Mn AOS): 3.947 | | | |

**Table S2.** The specific surface area and suspension densities of the reactants.

| Name | Concentration (mg/L) | Specific surface area, SSA ($m^2$/g) | Suspension densities ($m^2$/L) |
|---|---|---|---|
| Cr(OH)$_3$ | 500 | 103.24 | 51.62 |
| δ-MnO$_2$ | 10 | 88.35 | 0.8835 |

**Table S3.** Cr(VI) and Mn(II) concentrations in adsorption experiments at pH 9, 10, and 11, respectively.

| mg/L | pH=9 | pH=10 | pH=11 |
|---|---|---|---|
| Cr(VI) in Cr(OH)$_3$ suspension | | | |
| Initial concentration | 0.502 | 0.507 | 0.501 |
| Final concentration | 0.472 | 0.468 | 0.494 |
| Adsorption capacity | 0.03 | 0.048 | 0.007 |
| Cr(VI) in MnO$_2$ suspension | | | |
| Initial concentration | 0.502 | 0.507 | 0.501 |
| Final concentration | 0.478 | 0.474 | 0.480 |
| Adsorption capacity | 0.034 | 0.043 | 0.031 |
| Mn(II) in MnO$_2$ suspension | | | |
| Initial concentration | 10.09 | 10.09 | 10.09 |
| Final concentration | 0.7759 | 0.5573 | 0.0203 |
| Adsorption capacity | 9.3141 | 9.5327 | 10.0697 |

When Cr(OH)$_{3(s)}$ and δ-MnO$_{2(s)}$ were added in the NaCr$_2$O$_4$ solution at different pH (9-11), the Cr(VI) concentration in each solution was near to initial Cr(VI) concentration. However, when δ-MnO$_{2(s)}$ was added in to the Mn(NO$_3$)$_2$ solution at different pH, the Mn(II) concentration in each solution was determined much less than initial Mn(II) concentration. The results indicated that the absorption of Cr(VI) was almost negligible onto both Cr(OH)$_{3(s)}$ and δ-MnO$_2$ solids, whereas Mn(II) was strongly adsorbed on the surface of δ-MnO$_2$ solids.

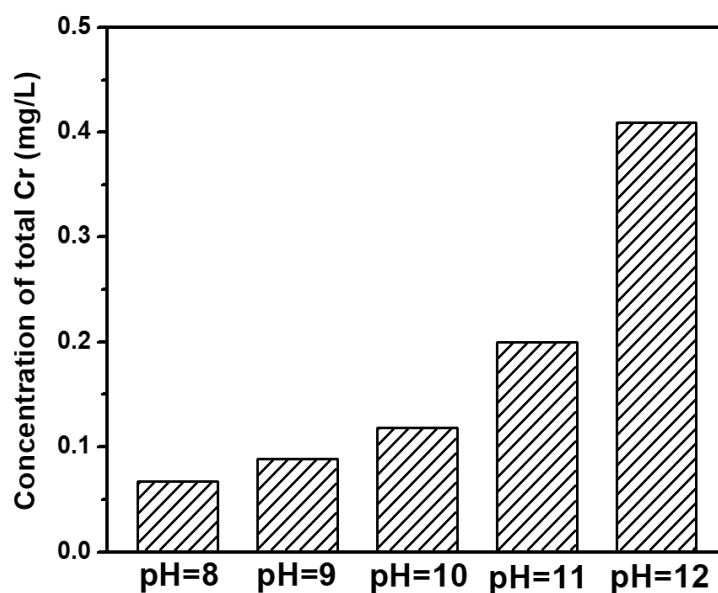## 2.2 Cr(OH)₃ dissolution in alkaline solution



**Figure S3.** Total concentration of dissolved Cr from $Cr(OH)_{3(s)}$ within 96 hours in anoxic condition with pH values range from 8 to 12. The initial concentration of $Cr(OH)_3$ is 500 mg/L.

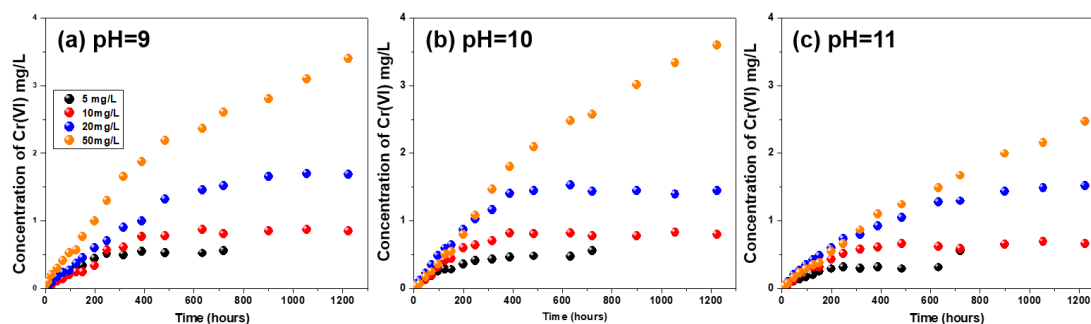## 2.3 Cr(OH)₃ oxidation with different concentrations of δ-MnO₂ under anoxic condition



**Figure S4.** Cr(VI) generation due to the reactions between 500 mg/L $Cr(OH)_3$ and different concentrations of δ-MnO₂ at pH (a) 9, (b) 10, and (c) 11 under anoxic conditions. The initial MnO₂ suspension concentration was 5 (black points), 10 (red points), 20 (blue points) and 50 mg/L (orange points).

## 2.4 Oxidation of Cr(OH)₃ with Mn(II) as a catalyst

As shown in Figure S5, 20 mM Mn(NO₃)₂ stock solution under oxic condition became to a suspension when the pH was adjusted to 9-11, and after standing for 3 minutes the solid settlement was formed. The XRD patterns of solid products show that hausmannite (Mn₃O₄) and feitknechtite (β-MnOOH) were

formed at pH 9-10 and mainly hausmannite formed at pH 11, implying that Mn(II) was oxidized to form Mn(III, IV) oxides. Table S4 shows that the concentration of Mn(II) in solution obviously decreased with higher pH, indicating that more Mn(II) was oxidized to form Mn(III, IV) oxides. In contrast, the oxidation of Mn(II) to Mn(III/IV) oxides under common environmental pH and Eh conditions is very slow kinetically because of the unfavorable high energetics of the aqueous-phase half-reaction (i.e. Mn(II) – $e^-$ =Mn(III), $\varphi^{\theta}$ = 1.54 eV, and Mn(II) - $2e^-$ + $2H_2O$ = Mn(IV)$O_2$ + $4H^+$, $\varphi^{\theta}$ = 1.22 eV).[8] It implies that the generation of Cr(VI) under alkaline condition could be ascribed to the newly formed Mn(III, IV) oxides (Pathway 3). However, the formation of Mn(III, IV) oxides was not identifiable in the simulated system of rCOPR due to the low content (Figure S6). To demonstrate this hypothesis, an experiment with Cr(OH)$_3$ and aqueous Mn(II) at a similar concentration ratio (500 mg/L Cr(OH)$_3$ suspension with 0.2 mM Mn(NO$_3$)$_2$) under oxic conditions was conducted. The XRD patterns of solid products (Figure S7) show that the products have poor crystallinity and it is difficult to obtain the qualitative information about Mn species through XRD analysis. In addition, it is difficult to avoid the peaks at 18.4°, due to the stir bars after long-term experiments. Although the newly formed Mn(III, IV) oxides were not identifiable by XRD, the SEM images (Figure S8) show that the solid products were likely hausmannite (Mn$_3$O$_4$) and/or feitknechtite (β-MnOOH) with characteristic floccules and fibrous in strips, respectively.[7,8] Moreover, by SEM observation it was found that most of the manganese oxides transformed into hausmannite (Mn$_3$O$_4$) while a smaller amount of feitknechtite (β-MnOOH) was formed.



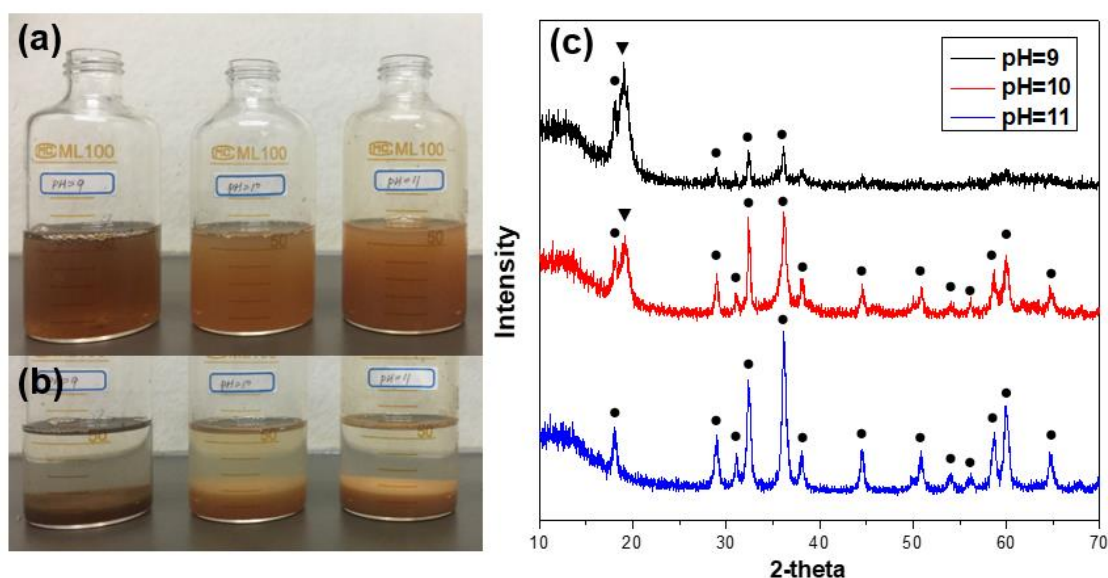**Figure S5.** The pictures of (a) the suspension and (b) that after standing for 3 minutes. (c) XRD patterns of the solid products in 20 mM Mn(NO$_3$)$_2$ stock solution with different pH (9-11) under oxic condition.

The main peaks indicated as "●" is hausmannite ($Mn_3O_4$) and "▼" is feitknechtite (β-MnOOH).

**Table S4.** Concentration of Mn(II) at different solution pH (9-11), 20 mM $Mn(NO_3)_2$ stock solution under oxic condition

| mg/L | pH=9 | pH=10 | pH=11 |
|---|---|---|---|
| Initial concentration | 100.92 | 100.92 | 100.92 |
| Final concentration | 84.2654 | 36.2668 | 8.7125 |
| Decrease | 16.6546 | 64.6532 | 92.2075 |
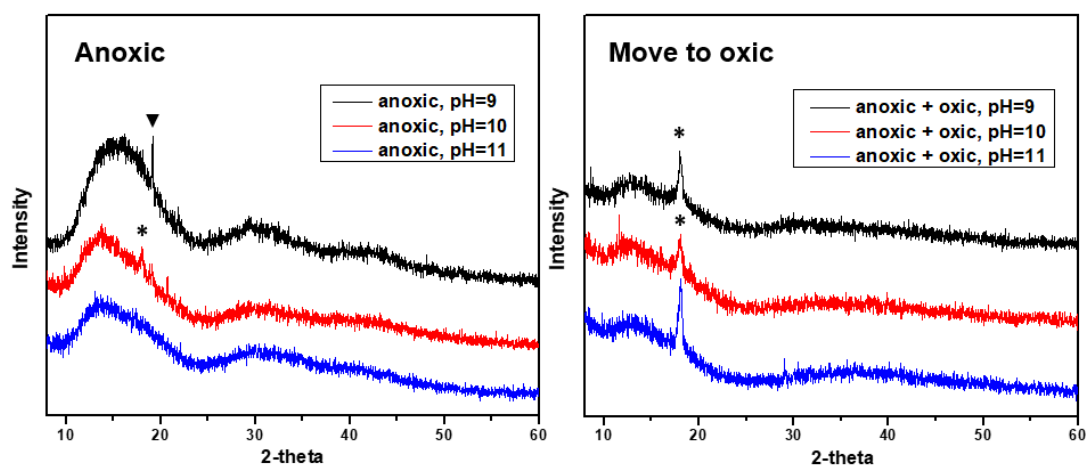


**Figure S6.** XRD patterns of solid products from the simulated system of rCOPR (500 mg/L $Cr(OH)_3$ and 10 mg/L δ-$MnO_2$) at pH 9, 10, and 11 under (a) anoxic condition for 1,224 h, and (b) after anoxic experiment and then placed in the atmospheric environment for 1,224 h. The main peaks ($2\theta=18.4°$) are indicated as "*", which may due to the stir bars. And the peaks at ($2\theta=19.2°$) indicated as "▼" is feitknechtite (β-MnOOH).
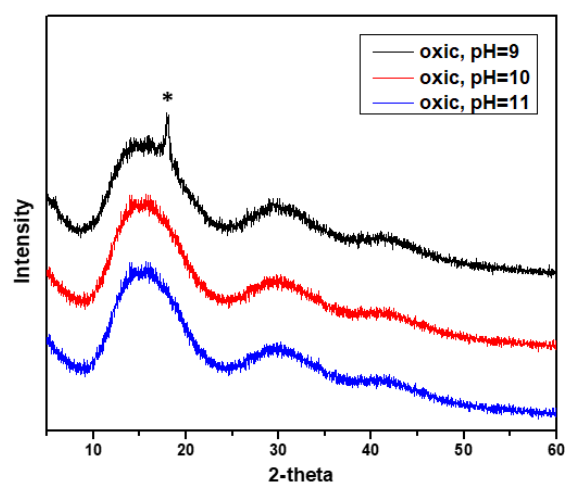
**Figure S7.** XRD patterns of the solid products from 500 mg/L $Cr(OH)_3$ suspension with 0.2 mM $Mn(NO_3)_2$ under oxic condition for 400h at pH 9, 10, and 11, respectively. The main peaks are indicated as "*" due to the stir bars.
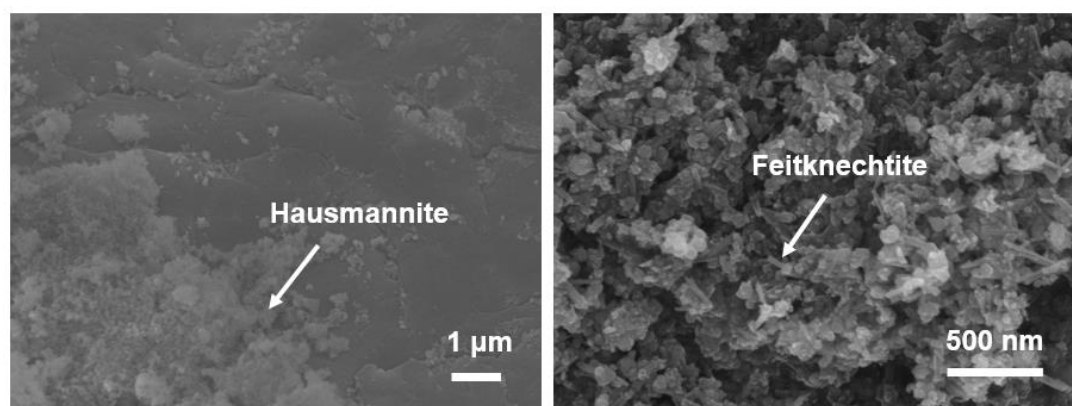


**Figure S8.** SEM photos of the solid products from the interaction between 500 mg/L $Cr(OH)_3$ and 0.2 mM $Mn(NO_3)_2$ under oxic condition at pH 11. Similar morphologies were also observed at pH 9 and 10.

## 2.5 Products analysis
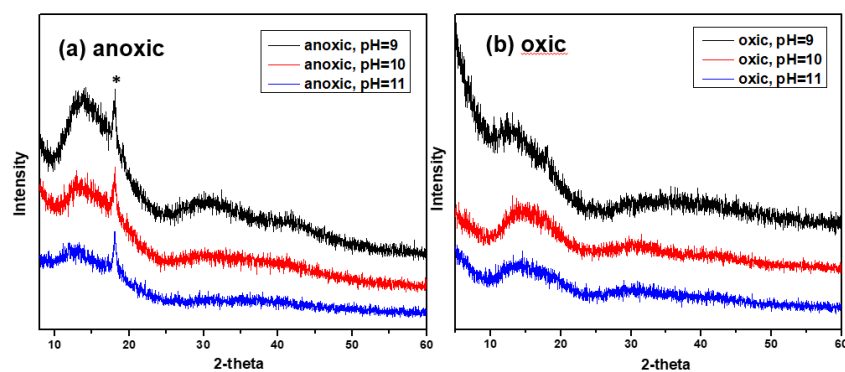
**Figure S9.** XRD patterns of solid products in 500 mg/L Cr(OH)$_3$ suspension under (a) anoxic condition and (b) oxic condition for 2,112 h (88 days) at pH 9, 10, and 11, respectively. The products maintain poor crystallinity and the main peaks are indicated as "*", which may due to the stir bars.
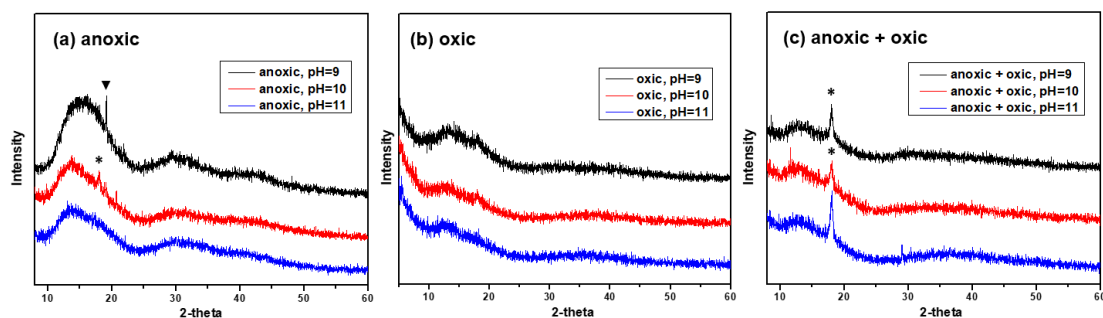
**Figure S10.** XRD patterns of solid products from the interaction between 500 mg/L Cr(OH)$_3$ and 10 mg/L δ-MnO$_2$ at pH 9, 10, and 11, respectively, under (a) anoxic condition for 1,224 h, (b) oxic condition for 3,811 h; (c) XRD patterns of the solid products of the suspension after anoxic experiments and then moved to the atmospheric environment at 1,224 h. The main peaks (2θ=18.4°) are indicated as "*", which may due to the stir bars. And the peaks at (2θ=19.2°) indicated as "▼" is feitknechtite (β-MnOOH). The XRD patterns show that most of the products remained poor crystallinity. The broad humps at 14.2° (2θ), indicating a lot of residual Cr(OH)$_{3(s)}$ after anoxic condition which gradually disappeared under oxic condition due to greater oxidation degree.

**Figure S11.** XPS spectra of Mn 2p$_{3/2}$ photoelectron lines for the solid products.

**Table S5**. Summary of the percentages of Mn(II), Mn(III), and Mn(IV) products using XPS Mn $2p_{3/2}$.

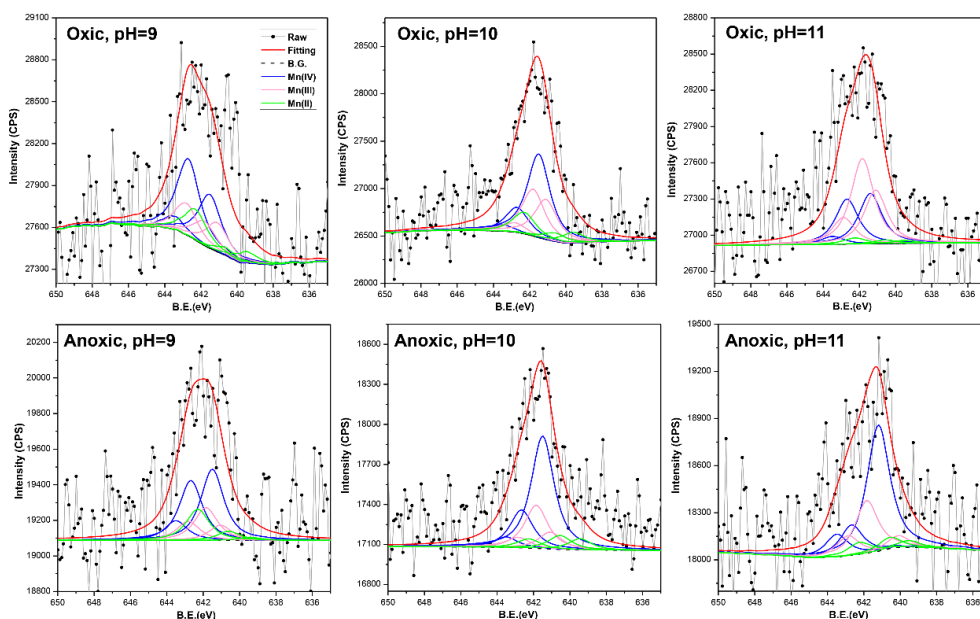| Percent | Anoxic condition ($\delta$-MnO$_2$) | | | Oxic condition ($\delta$-MnO$_2$) | | |
|---|---|---|---|---|---|---|
| (%) | pH 9 | pH 10 | pH 11 | pH 9 | pH 10 | pH 11 |
| Mn(IV) | 59.5 | 60.0 | 57.8 | 34.5 | 45.6 | 49.5 |
| Mn(III) | 28.3 | 26.2 | 25.3 | 54.9 | 38.1 | 29.6 |
| Mn(II) | 12.2 | 13.8 | 16.9 | 10.6 | 16.2 | 20.9 |

**Table S6.** Binding energies (BE) of surface Mn species for fitting the Mn$2p_{3/2}$ peak of the solid products and the relative area of each multiplet for the surface species.

**Products at pH 9.0**

| anoxic condition | | | | oxic condition | | |
|---|---|---|---|---|---|---|
| surface species | BE (eV) | FWHM (eV) | Percent (%) | BE (eV) | FWHM (eV) | Percent (%) |
| Mn(IV)-O multiplet 1 | 641.49 | 1.5 | 27.18 | 641.51 | 1.5 | 19.30 |
| Mn(IV)-O multiplet 2 | 642.67 | 1.5 | 22.87 | 642.70 | 1.5 | 27.56 |
| Mn(IV)-O multiplet 3 | 643.50 | 1.5 | 7.73 | 643.50 | 1.5 | 4.82 |
| Mn(IV)-O multiplet 4 | 644.72 | 1.5 | 0.04 | 644.58 | 1.5 | 0.01 |
| Mn(IV)-O multiplet 5 | 645.75 | 1.5 | 0.00 | 645.60 | 1.5 | 0.08 |
| **Mn(IV)-O overall: 57.82 (%)** | | | | **Mn(IV)-O overall: 51.77 (%)** | | |
| Mn(III)-O multiplet 1 | 640.30 | 1.5 | 0.12 | 640.30 | 1.5 | 0.00 |
| Mn(III)-O multiplet 2 | 641.50 | 1.5 | 5.75 | 641.11 | 1.5 | 10.44 |
| Mn(III)-O multiplet 3 | 641.85 | 1.5 | 12.40 | 641.81 | 1.5 | 8.70 |
| Mn(III)-O multiplet 4 | 642.82 | 1.5 | 7.28 | 642.81 | 1.5 | 11.18 |
| Mn(III)-O multiplet 5 | 644.24 | 1.5 | 0.02 | 644.20 | 1.5 | 0.00 |
| **Mn(III)-O overall: 25.57 (%)** | | | | **Mn(III)-O overall: 30.31 (%)** | | |
| Mn(II)-O multiplet 1 | 639.45 | 1.5 | 1.22 | 639.50 | 1.5 | 3.91 |

| | | | | | | |
|---|---|---|---|---|---|---|
| Mn(II)-O multiplet 2 | 640.60 | 1.5 | 3.50 | 640.61 | 1.5 | 2.81 |
| Mn(II)-O multiplet 3 | 641.45 | 1.5 | 0.08 | 641.40 | 1.5 | 0.04 |
| Mn(II)-O multiplet 4 | 642.33 | 1.5 | 11.80 | 642.32 | 1.5 | 11.04 |
| Mn(II)-O multiplet 5 | 643.82 | 1.5 | 0.01 | 643.82 | 1.5 | 0.11 |
| **Mn(II)-O overall: 16.61 (%)** | | | | **Mn(II)-O overall: 17.92 (%)** | | |

**Products at pH 10.0**

| anoxic condition | | | | oxic condition | | |
|---|---|---|---|---|---|---|
| surface species | BE (eV) | FWHM (eV) | Percent (%) | BE (eV) | FWHM (eV) | Percent (%) |
| Mn(IV)-O multiplet 1 | 641.20 | 1.5 | 42.37 | 641.51 | 1.5 | 33.13 |
| Mn(IV)-O multiplet 2 | 642.68 | 1.5 | 14.15 | 642.72 | 1.5 | 9.94 |
| Mn(IV)-O multiplet 3 | 643.48 | 1.5 | 4.01 | 643.50 | 1.5 | 2.55 |
| Mn(IV)-O multiplet 4 | 644.58 | 1.5 | 0.12 | 644.58 | 1.5 | 0.00 |
| Mn(IV)-O multiplet 5 | 645.60 | 1.5 | 0.04 | 645.60 | 1.5 | 0.00 |
| **Mn(IV)-O overall: 60.69 (%)** | | | | **Mn(IV)-O overall: 45.62 (%)** | | |
| Mn(III)-O multiplet 1 | 640.30 | 1.5 | 0.08 | 640.30 | 1.5 | 0.09 |
| Mn(III)-O multiplet 2 | 641.15 | 1.5 | 6.17 | 641.11 | 1.5 | 15.81 |
| Mn(III)-O multiplet 3 | 641.83 | 1.5 | 16.20 | 641.81 | 1.5 | 18.55 |
| Mn(III)-O multiplet 4 | 642.88 | 1.5 | 3.93 | 642.81 | 1.5 | 3.66 |
| Mn(III)-O multiplet 5 | 644.20 | 1.5 | 0.01 | 644.20 | 1.5 | 0.02 |
| **Mn(III)-O overall: 26.48 (%)** | | | | **Mn(III)-O overall: 38.14 (%)** | | |
| Mn(II)-O multiplet 1 | 639.52 | 1.5 | 4.14 | 639.50 | 1.5 | 4.25 |
| Mn(II)-O multiplet 2 | 640.57 | 1.5 | 5.23 | 640.61 | 1.5 | 3.40 |
| Mn(II)-O multiplet 3 | 641.40 | 1.5 | 0.00 | 641.40 | 1.5 | 0.00 |
| Mn(II)-O multiplet 4 | 642.31 | 1.5 | 3.46 | 642.32 | 1.5 | 8.52 |
| Mn(II)-O multiplet 5 | 643.80 | 1.5 | 0.00 | 643.82 | 1.5 | 0.07 |
| **Mn(II)-O overall: 12.83 (%)** | | | | **Mn(II)-O overall: 16.24 (%)** | | |

**Products at pH 11.0**

| anoxic condition | | | | oxic condition | | |
|---|---|---|---|---|---|---|
| surface species | BE (eV) | FWHM (eV) | Percent (%) | BE (eV) | FWHM (eV) | Percent (%) |
| Mn(IV)-O multiplet 1 | 641.49 | 1.5 | 43.37 | 641.39 | 1.5 | 28.42 |
| Mn(IV)-O multiplet 2 | 642.67 | 1.5 | 10.32 | 642.68 | 1.5 | 18.59 |
| Mn(IV)-O multiplet 3 | 643.51 | 1.5 | 8.01 | 643.48 | 1.5 | 2.51 |
| Mn(IV)-O multiplet 4 | 644.58 | 1.5 | 0.10 | 644.58 | 1.5 | 0.20 |
| Mn(IV)-O multiplet 5 | 645.70 | 1.5 | 0.02 | 645.6 | 1.5 | 0.01 |
| **Mn(IV)-O overall: 61.82 (%)** | | | | **Mn(IV)-O overall: 49.73 (%)** | | |
| Mn(III)-O multiplet 1 | 640.30 | 1.5 | 0.11 | 640.30 | 1.5 | 0.05 |
| Mn(III)-O multiplet 2 | 641.50 | 1.5 | 2.90 | 641.10 | 1.5 | 12.81 |
| Mn(III)-O multiplet 3 | 641.85 | 1.5 | 18.06 | 641.83 | 1.5 | 23.51 |
| Mn(III)-O multiplet 4 | 642.82 | 1.5 | 6.78 | 642.88 | 1.5 | 9.03 |
| Mn(III)-O multiplet 5 | 644.22 | 1.5 | 0.00 | 644.20 | 1.5 | 0.00 |
| **Mn(III)-O overall: 27.85 (%)** | | | | **Mn(III)-O overall: 45.41 (%)** | | |
| Mn(II)-O multiplet 1 | 639.45 | 1.5 | 2.30 | 639.52 | 1.5 | 1.07 |
| Mn(II)-O multiplet 2 | 640.61 | 1.5 | 3.79 | 640.57 | 1.5 | 1.30 |
| Mn(II)-O multiplet 3 | 641.42 | 1.5 | 0.13 | 641.4 | 1.5 | 0.00 |
| Mn(II)-O multiplet 4 | 642.31 | 1.5 | 4.11 | 642.24 | 1.5 | 2.50 |
| Mn(II)-O multiplet 5 | 643.80 | 1.5 | 0.01 | 643.8 | 1.5 | 0.00 |
| **Mn(II)-O overall: 10.33 (%)** | | | | **Mn(II)-O overall: 4.87 (%)** | | |

**2.6 Kinetic model establishment**

Kinetic models were established based on constraints of mass balances and the stoichiometry of the redox reactions to clarify the oxidation rates of $Cr(OH)_3$ under anoxic and oxic conditions. The temperature, solution pH, atmospheric pressure, and ionic strength, which is generally related to its solubility,[9,10] were almost the same throughout the experiments. The initial amount of $Cr(OH)_3$ (mg/L) was 50 times as the amount of $\delta$-$MnO_2$ and less than 10% of total Cr(III) was finally consumed, indicating that the content of dissolved Cr(III) kept a constant and was sufficient for the oxidation. Therefore, the equilibrium concentration of $Cr(OH)_3$ was assumed to be constant. An overview conceptual model that describes the

processes occurring is presented in Figure S12. As shown in Figure S12, the oxidation of Cr(III) includes three pathways: 1) direct oxidation by oxygen, 2) oxidation by δ-MnO$_2$, and 3) catalytic oxidation with MnO$_x$ formed in situ via Mn(II) oxidation by oxygen.
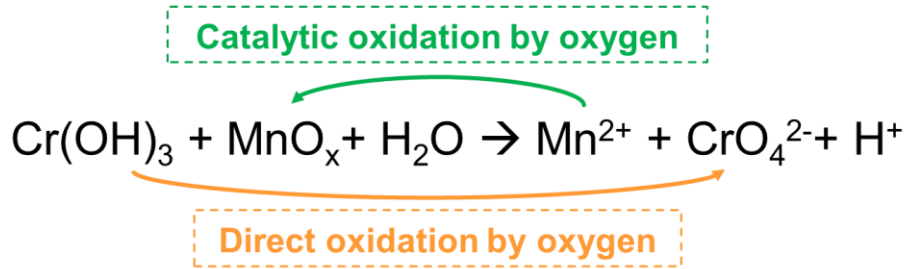
**Catalytic oxidation by oxygen**

$$Cr(OH)_3 + MnO_x + H_2O \rightarrow Mn^{2+} + CrO_4^{2-} + H^+$$

**Direct oxidation by oxygen**

**Figure S12**. Conceptual model of Cr(OH)$_3$ oxidation by MnO$_x$ considering the direct oxidation by oxygen, oxidation by the coexisting MnO$_x$ and the catalytic oxidation by MnO$_x$ formed via Mn(II) and oxygen. Both the coexisting MnO$_x$ and the newly formed MnO$_x$ can oxidize Cr(OH)$_3$ and produce toxic Cr(VI). The MnO$_x$ shown here is a collective name of manganese oxides, referring to the coexisting MnO$_x$ (δ-MnO$_2$) and the newly formed products (i.e., Mn$_3$O$_4$ and MnOOH in this study).

As described in the section of "3.3 Kinetics model for Cr(III) oxidation" in main text, the specific rate equations are as follows:

$$-\frac{d(Cr(VI)_{Path\ 1})}{dt} = k_1[Cr(III)_{diss}] = k_1' \qquad (Eq.\ 1)$$

$$-\frac{d(Cr(VI)_{Path\ 2})}{dt} = k_2[\delta - MnO_2][Cr(III)_{diss}] = k_2'[\delta - MnO_2] \qquad (Eq.\ 2)$$

$$-\frac{d(Cr(VI)_{overall})}{dt} = k_1[Cr(III)_{diss}] + k_2[\delta - MnO_2][Cr(III)_{diss}] + k_3[MnO_x][Cr(III)_{diss}] (Eq.\ 3)$$

$$[MnO_x] = \gamma[Mn^{2+}] \qquad (Eq.\ 4)$$

$$[Mn^{2+}] = \eta[\delta - MnO_2] \qquad (Eq.\ 5)$$

$$-\frac{d(Cr(VI))}{dt} = k_1' + k_2'[\delta - MnO_2] + k_3'[\delta - MnO_2][Cr(III)_{diss}] \qquad (Eq.\ 6)$$

where $k_1$, $k_2$, and $k_3$ are the rate constants of Cr(VI) oxidation; $k_1'$, $k_2'$, and $k_3'$ are the apparent rate constants in Pathways 1, 2, and 3, respectively. According to Eq. 1 to Eq. 6, $k_1'$, $k_2'$, and $k_3'$ were the apparent constants in Pathways 1, 2, and 3, respectively. $k_1'$ was derived from the data in Figure 1b, and the optimized fitting data at different pH showed in Figure S13. While $k_2'$ was derived from the data in Figure 2a (within 400 h before plateau), where the oxidizing agent of Cr(III) was only δ-MnO$_2$, and the optimized fitting data at different pH showed in Figure S14. We chose the data in Figure 2b with

a reaction time greater than 1500 hours for deriving $k_3'$ because during this period pathway 2 has almost stabilized and the contribution of pathway 3 was more prominent. The optimized fitting data of $k_3'$ was calculated using MATLAB by multiplying $k_1'$ and $k_2'$. To test the reliability of the results, the fitting data using the kinetics model in Eq. 6 were showed in Figure 2b with minimum coefficients ($R^2$) of determination greater than 0.88.
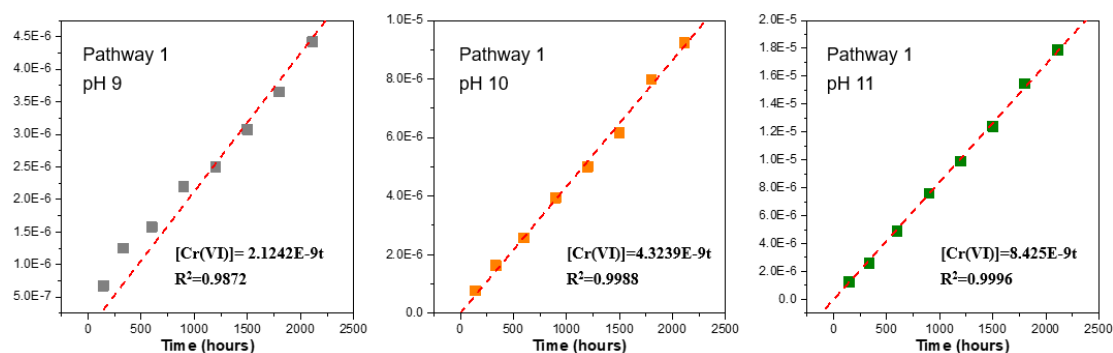


**Figure S13.** The rates of Cr(VI) generation in Pathway 1. The experimental results are shown as solid square and the fitting data are shown as dash lines. The minimum coefficients ($R^2$) of determination were inserted.



**Figure S14.** The rates of Cr(VI) generation in Pathway 2. The experimental results are shown as solid square and the fitting data are shown as dash lines. The minimum coefficients ($R^2$) of determination were inserted.
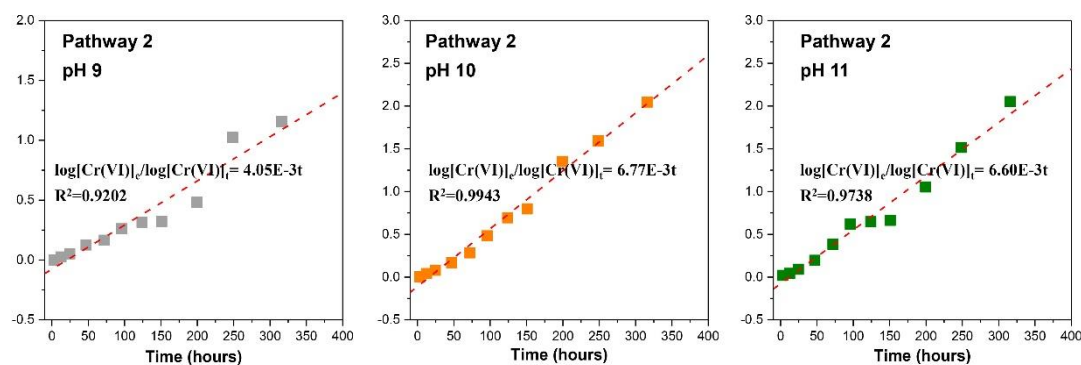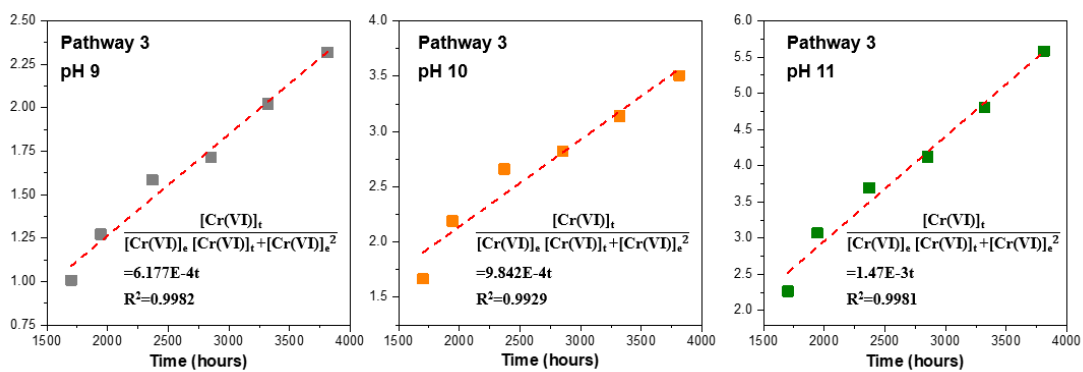
**Figure S15.** The rates of Cr(VI) generation in Pathway 3. The experimental results are shown as solid square and the fitting data are shown as dash lines. The optimized fitting data of Pathway 3 was solved by MATLAB using the difference between the rates in the overall reaction and that in Pathway 1&2.

It was found that $k_1'$ at pH 9, 10, and 11 were $2.12 \times 10^{-9}$, $4.32 \times 10^{-9}$, and $8.42 \times 10^{-9}$ M h$^{-1}$, respectively, with minimum coefficients ($R^2$) of determination more than 0.987. Although the rate constants in Pathway 1 ($k_1'$) increased with increasing pH, Cr(VI) was generated slowly. In contrast, $k_2'$ for Pathway 2 was $4.05 \times 10^{-3}$, $6.77 \times 10^{-3}$, and $6.60 \times 10^{-3}$ h$^{-1}$ for pH 9, 10, and 11, respectively, almost six orders of magnitude greater than $k_1'$. Interestingly, the rates of the Cr(III) catalytic oxidation by MnO$_x$ ($k_3'$) were $6.18 \times 10^{-4}$, $9.84 \times 10^{-4}$, and $1.47 \times 10^{-3}$ M$^{-1}$ h$^{-1}$ at pH 9, 10, and 11, respectively. $k_3'$ was on a similar order of magnitude as $k_2'$, suggesting great potential for effective oxidation via Pathway 3, especially at higher pH.

It needs to be noted that, Cr(OH)$_3$ was sufficient throughout the experiment and it only consumed about 10% to produce toxic Cr(VI). Therefore, the [Cr(III)$_{diss}$] was simplified to a constant in these models (Eq. 1 and Eq. 2). This simplification might ignore the influence of the Cr(III)-reactants on the rate of Cr(VI) formation. Moreover, we replaced [MnO$_x$] with [MnO$_2$] with correction coefficients (Eq. 6) because MnO$_x$ generated in situ was difficult to precisely quantify and it was proportional to δ-MnO$_2$ (Eq. 4 and 5). As the correction coefficients in Eq. 4 and 5 was regard as a constant, we would ignore the acceleration of the mass transfer rate during the reaction and the catalysis by the presence of solid particles.

## 2.7 Influence of the surface area of reactant solid

The surface area of the reactant solid as one of the controlling factors for the oxidation of $Cr(OH)_{3(s)}$ needs to be considered. The BET specific surface areas of $Cr(OH)_{3(s)}$ and $\delta$-$MnO_{2(s)}$ are 103.24 and 88.35 $m^2/g$, respectively. In addition, the $Cr(OH)_{3(s)}$ and $\delta$-$MnO_{2(s)}$ have poor crystallinity, indicating sufficient surface active sites. The relative contributions of the three pathways were calculated based on the results in Figure 1 (500 mg/L $Cr(OH)_3$ suspension) and Figure 2 (500 mg/L $Cr(OH)_3$ suspension with 10 mg/L $\delta$-$MnO_2$). The total surface area of the reactant solid for the first batch experiment is 51.62 $m^2/L$ and for the second is 52.50 $m^2/L$, and the former accounts for 98.32% of the latter. The contribution from pathway 1 was calculated by the results in Figure 1b under oxic condition, which can be effected by the surface area of $Cr(OH)_{3(s)}$. The contribution from pathway 2 was calculated by the results in Figure 2a under anoxic condition, which theoretically depends on the surface area of $\delta$-$MnO_{2(s)}$. However, the oxidation ceased when the Cr(VI) concentration reached 0.67-0.85 mg/L, ~ 40% of the theoretical value, even though the reactants were sufficient for further oxidation. It means that the contribution from pathway 2 did not make full use of the surface area of $\delta$-$MnO_{2(s)}$. The contribution from pathway 3 was calculated by the results in Figure 2b under oxic condition minus the contributions from pathway 1 and 2, which can be influenced by the surface area of both $Cr(OH)_{3(s)}$ and $\delta$-$MnO_{2(s)}$. It can be found that the effects of the surface area of $Cr(OH)_{3(s)}$ and $\delta$-$MnO_{2(s)}$ on the three pathways of Cr(III) oxidation are complicated and it is difficult to distinguish the precise influence of the surface area of $Cr(OH)_{3(s)}$ and/or $\delta$-$MnO_{2(s)}$ on the rate of Cr(VI) generation in each pathway. Overall, the more surface area of the reactant solid should improve the rate of Cr(VI) generation. Therefore, the apparent rate constants in pathway 1, 2, and 3 ($k_1'$, $k_2'$, and $k_3'$) are used to describe the rates of Cr(VI) generation in each pathway, which include the influences of the specific surface area, stirring rate, ion strength and so on.

## References

(1) Lee, G.; Hering, J.G. Oxidative Dissolution of Chromium(III) Hydroxide at pH 9, 3, and 2 with Product Inhibition at pH 2. *Environ. Sci. Technol.* **2005**, *39*(13), 4921-4928.

(2) Villalobos, M.; Toner, B.; Bargar, J.; Sposito, G. Characterization of the manganese oxide produced by pseudomonas putida strain MnB1. *Geochim. Cosmochim. Ac.* **2003**, *67*(14), 2649-2662.

(3) Liu, C.S.; Zhang, L.J.; Feng, C.H.; Wu, C.A.; Li, F.B.; Li, X.Z. Relationship between oxidative degradation of 2-mercaptobenzothiazole and physicochemical properties of manganese (hydro)oxides.

*Environ. Chem.* **2009**, *6*(1), 83.

(4) Nesbitt, H.W.; Banerjee, D. Interpretation of XPS Mn(2p) spectra of Mn oxyhydroxides and constraints on the mechanism of $MnO_2$ precipitation. *Am. Mineral.* **1998**, *83*(3), 305-315.

(5) Lefkowitz, J.P.; Rouff, A.A.; Elzinga, E.J. Influence of pH on the Reductive Transformation of Birnessite by Aqueous Mn(II). *Environ. Sci. Technol.* **2013**, *47*(18), 10364-10371.

(6) Ravel, B.; Newville, M. ATHENA, ARTEMIS, HEPHAESTUS: data analysis for X-ray absorption spectroscopy using IFEFFIT. *Journal of Synchrotron Radiation.* **2005**, *12*(4), 537-541.

(7) Peng, X.; Ichinose, I. Green-Chemical Synthesis of Ultrathin β-MnOOH Nanofibers for Separation Membranes. *Adv. Funct. Mater.* **2011**, *21*(11), 2080-2087.

(8) Lan, S.; Wang, X.; Xiang, Q.; Yin, H.; Tan, W.; Qiu, G.; Liu, F.; Zhang, J.; Feng, X. Mechanisms of Mn(II) catalytic oxidation on ferrihydrite surfaces and the formation of manganese (oxyhydr)oxides. *Geochim. Cosmochim. Ac.* **2017**, *211*, 79-96.

(9) Rai, D.; Moore, D.A.; Hess, N.J.; Rosso, K.M.; Rao, L.; Heald, S.M. Chromium(III) Hydroxide Solubility in the Aqueous $K^+$-$H^+$-$OH^-$-$CO_2$-$HCO_3^-$ -$CO_3^{2-}$ -$H_2O$ System: A Thermodynamic Model. *J. Solution Chem.* **2007**, *36*(10), 1261-1285.

(10) Ziemniak, S.E.; Jones, M.E.; Combs, K.E.S. Solubility and Phase Behavior of Cr(III) Oxides in Alkaline Media at Elevated Temperatures. *J. Solution Chem.* **1998**, *27*(1), 33-66.